Triaxiality in the proton emitter ^{109}I

Swati Modi, M. Patial,* and P. Arumugam†
Department of Physics, Indian Institute of Technology Roorkee, Roorkee 247667, India

E. Maglione
Dipartimento di Fisica e Astronomia "G. Galilei", and Istituto Nazionale di Fisica Nucleare, Via Marzolo 8, I-35131 Padova, Italy

L. S. Ferreira
Centro de Física e Engenharia de Materiais Avançados CeFEMA, and Departmento de Física, Instituto Superior Técnico, Universidade de Lisboa, Avenida Rovisco Pais, P1049-001 Lisbon, Portugal

(Received 20 March 2017; published 25 May 2017)

We study the role of triaxial deformation in the proton-emitting nucleus ^{109}I. We analyze the rotational spectrum as well as the decay width within the nonadiabatic quasiparticle approach. The parent nuclear wave functions are calculated using a modified rotation-particle coupling where the matrix elements of the Hamiltonian representing the rotational states of the parent nucleus are written in terms of the rotational energies of the daughter nucleus. The measured spectrum of the daughter nucleus ^{108}Te suggests a strong role of either triaxial or vibrational degrees of freedom which is applicable for ^{109}I also. With these results we successfully explain the spectra of the parent and daughter and also the decay width in a unified way which enables us to establish the configuration of the rotational bands and the decaying state.

DOI: 10.1103/PhysRevC.95.054323

I. INTRODUCTION

The spontaneous proton emission from ^{109}I was observed for the first time in 1984 [1]. ^{109}I lies near the double shell closure ($Z = N = 50$), which forms the island of α and proton emission. ^{109}I is preponderantly a proton emitter [1,2], but it has also a small branch $(1.4 \pm 0.4) \times 10^{-4}$ [3] of α emission. The interpretation of these decays and the knowledge of the nuclear structure properties of ^{109}I will be quite important to the understanding of astrophysical events [3]. Knowledge of the Q value for the α decay of ^{109}I allows the determination of the Q value of proton emission from ^{105}Sb [3]. ^{105}Sb takes part in the Sn-Sb-Te cycle, which burns hydrogen through the rapid proton-capture process and gives rise to type 1 x-ray bursts. ^{109}I is proposed to be a ground-state proton emitter, but the exact proton decaying state is not assigned yet. Many of the theoretical calculations within the strong coupling limit have suggested the $\Omega^{\pi} = 1/2^{+}$ [4–6] state of the $g_{7/2}$ orbital as the ground state, where Ω is the z projection of the total angular momentum of the single particle. Microscopic calculation [6] of the half-life for proton emission from ^{109}I in the strong coupling limit and the nonadiabatic method based on the coupled-channel Schrödinger equation [7] also predicted the same decaying state, but with a slightly different quadrupole deformation of $\beta_2 = 0.14$ and $\beta_2 = 0.10$, respectively. Within the relativistic Hartree-Bogoliubov model the proton decaying state is calculated as the $\Omega = 3/2^{+}$ [8] state of the $d_{5/2}$ orbital. On the experimental side, from the observation and measurements of the energy levels and half-life for proton emission, it was suggested that the $5/2^{+}$ state [3,9,10] coming from the $d_{5/2}$ is the ground state. The γ transitions proposed in Refs. [11,12] show some discrepancies but the positive and negative parity yrast bands were further revised in [10,13]. This revision of γ transitions [10] and further analysis with the cranked shell model suggested a triaxial deformation, also consistent with the predictions of macroscopic-microscopic calculations [14]. So far, the role of triaxiality has been ignored while calculating the proton emission half-life of ^{109}I.

Here we apply the nonadiabatic quasiparticle approach [15] in which the structure and decay properties of triaxially deformed proton emitters can be investigated by the coupling of the rotor energies directly with the particle states. This is a modified form of the conventional particle-rotor model (PRM) [16–19] where the rotor spectrum may deviate from the rotational spectrum of a rigid rotor. In the following sections, we discuss our theoretical framework and its application to studying proton emission from ^{109}I and its rotational spectra.

II. THEORETICAL FRAMEWORK

The properties of a triaxial proton emitter is studied with the microscopic nonadiabatic coupling of the quasiparticle (in a triaxial mean field) and the triaxial rotor. The total Hamiltonian for the particle-plus-rotor system is given by

$$H = H_{\text{avg}} + H_{\text{pair}} + H_{\text{rot}}, \tag{1}$$

where H_{avg} and H_{pair} correspond to the deformed mean field of the particles and the pairing interaction, respectively. $H_{\text{avg}} + H_{\text{pair}}$ gives the quasiparticle energy and H_{rot} is the triaxial rotor Hamiltonian given by

$$H_{\text{rot}} = \sum_{k=1,2,3} \frac{\hbar^2}{2\mathcal{I}_k} R_k^2. \tag{2}$$

Here $\mathcal{I}_k$ and R_k are the moments of inertia and angular momenta, respectively, in the three directions (1,2,3). The rotor

*Present address: Department of Physics, Worcester Polytechnic Institute, Worcester, Massachusetts 01609, USA.
†Corresponding author: p.arumugam@gmail.com

energies (E_{Ri}) corresponding to the above Hamiltonian can be expressed as

$$H_{\rm rot}|RM_Ri\rangle = E_{Ri}|RM_Ri\rangle, \tag{3}$$

with the eigenfunctions [20]

$$|RM_Ri\rangle = \sum_{K_R} c^{Ri}_{K_R}|RM_RK_R\rangle, \tag{4}$$

where the index M_R and K_R are the projections of R on the third axes in the laboratory frame (the z axes) and the intrinsic frame (the three axes) of the rotor, respectively, and i labels the different eigenstates for a given R. Since the nucleus need not be a rigid rotor, the above mentioned moments of inertia might not be constants. We consider the variable moment of inertia (VMI) given by [21]

$$\mathcal{I}_{kRi} = \mathcal{I}_{0Ri}\,\sin^2\left(\gamma - \frac{2\pi k}{3}\right). \tag{5}$$

The total energy can be written as (including the potential energy term [22])

$$E_{TRi} = \frac{1}{2}C(\mathcal{I}_{0Ri} - \mathcal{I}_0)^2 + \frac{1}{2\mathcal{I}_{0Ri}}\eta_{Ri}\ . \tag{6}$$

Here, $\eta_{Ri} = 2\mathcal{I}_{0Ri}E_{Ri}$ is a dimensionless quantity. C and $\mathcal{I}_0$ are the VMI parameters. The parameter C is related to the stiffness of the nucleus against vibrational degrees of freedom. The moment of inertia $\mathcal{I}_{0Ri}$ can be calculated [15] from the parameter $\mathcal{I}_0$ using the equilibrium condition for the total energy, $\partial E_{TRi}/\partial\mathcal{I}_{0Ri} = 0$. These parameters are calculated by fitting the theoretical energies E_{TRi} to the experimental energies. Thus we can calculate the total energies (6) as well as the wave functions for the rotor. This method [15] is an extension to the triaxial case, of the method given in Ref. [22] for the axially symmetric even-even rotor. The fitting of parameters C and $\mathcal{I}_0$ is done at every γ deformation. Hence the calculated rotor energies (fitted with experimental energies) will not have explicit dependence on the γ deformation.

To demonstrate the influence of γ deformation in a rotor spectrum, we use a simpler method where $\mathcal{I}_k$ is given by the hydrodynamical relation

$$\mathcal{I}_k = \mathcal{I}_0(R)\,\sin^2\left(\gamma - \frac{2\pi k}{3}\right),$$
$$\text{where}\quad \mathcal{I}_0(R) = \mathcal{I}_0\sqrt{1 + bR(R+1)}, \tag{7}$$

with the VMI parameter b [23]. $\mathcal{I}_0$ is calculated with the expression $\frac{\hbar^2}{2\mathcal{I}_0\sqrt{1+6b}} = \frac{E_{2+}}{6}$ [24]. b is related to the nonrigidity of the rotor. If $b = 0$, then the rotor is a pure rigid rotor and the moment of inertia does not depend on the angular momentum of the rotor.

The matrix element of the total Hamiltonian (1) for the particle-plus-rotor system in the K representation is given by

$$\langle q'K', IM|H|qK, IM\rangle = \epsilon_q\,\delta_{K'K}\delta_{q'q} + \sum_{lj\Omega_{p'}\Omega_p} W^{K'K}_{j\Omega_{p'}\Omega_p} \times \int dr\ f_{uv}\,\phi^{IK'*}_{lj\Omega_{p'}}(r)\,\phi^{IK}_{lj\Omega_p}(r), \tag{8}$$

where q specifies the single-particle state. K and M are the projections of the total angular momentum I on the three axes in the intrinsic frame and the z axis of the laboratory frame, respectively. The orbital and total angular momentum of the particle are given by l and j, respectively, and Ω_p is the projection of j on the third-axis in the intrinsic frame of the nucleus. ϵ_q are the quasiparticle energies given by

$$\epsilon_q = \sqrt{(e_q - \lambda)^2 + \Delta^2}, \tag{9}$$

where e_q are the single-particle energies and $\phi^{IK}_{lj\Omega_p}(r)$ are the single-particle wave functions calculated by using the Woods-Saxon potential along with the Coulomb and spin-orbit potentials [15]. The chemical potential λ is calculated through the BCS approach with the pairing gap fixed at $\Delta = 12/\sqrt{A}$ MeV. The matrix element between single-particle states is transformed to the matrix element between quasiparticle states by multiplying it with the factor $f_{uv} = (U_qU_{q'} + V_qV_{q'})$, where U_q and V_q are the BCS unoccupation and occupation probabilities, respectively. The transformation to quasiparticles enables us to identify the ground state configuration, since the yrast level naturally comes out to be the lowest in energy. The $W^{K'K}_{j\Omega_{p'}\Omega_p}$ are the matrix elements of $H_{\rm rot}$ in the K representation, which can be written as [15]

$$W^{K'K}_{j\Omega_{p'}\Omega_p} = \langle lj\Omega_{p'}K', IM|H_{\rm rot}|lj\Omega_pK, IM\rangle = \sum_{R,K_{R'},K_R} A^{IK'}_{j\Omega_{p'},RK_{R'}} \sum_i c^{Ri}_{K_{R'}}E_{TRi}c^{Ri}_{K_R}A^{IK}_{j\Omega_p,RK_R}, \tag{10}$$

with the transformation amplitude

$$A^{IK}_{j\Omega_p,RK_R} = \sqrt{\frac{2R+1}{2I+1}}\langle j\Omega_pRK_R|IK\rangle\sqrt{1+\delta_{K_R,0}}. \tag{11}$$

The rotational energies and the wave functions of the particle-plus-rotor system are calculated by diagonalizing the Hamiltonian (1). Hence we can have the one-quasiparticle rotational spectrum for the triaxial odd-A nucleus. The resulting wave functions are used in the calculation of the decay width and hence the half-life for proton emission.

The decay width is obtained from the overlap of initial (parent) and final-state wave functions. The final-state wave function is given by the coupling of the daughter nucleus and the outgoing proton wave function [25]. Thus the partial decay width for the triaxial odd-A nucleus is given by

$$\Gamma^{IR}_{lj} = \frac{2(2R+1)}{2I+1}\frac{\hbar^2\kappa}{\mu}\left|{\sum_{q,K,\Omega,K_R}}' g^{\tau}_{RK_R}\langle RK_Rj\Omega|IK\rangle \times a^I_{q,K}\,U^f_q\,\frac{\phi^{q\Omega}_{lj}(r)}{G_l(\kappa r) + iF_l(\kappa r)}\right|^2, \tag{12}$$

where κ is the wave vector of the emitting proton and μ is the reduced mass of the proton-core system. The prime on the summation denotes the constraint that $K - \Omega$ must be an even integer. For proton decay to the ground state of the daughter nucleus, $R = K_R = \tau = 0$ and $g^0_{0,0} = 1$. For the decay to the

lowest 2^+ state ($\tau = 1$)

$$g^1_{2,K_R} = \frac{1}{\sqrt{1+|K_R|/2}}\left[\frac{1}{2} + (-1)^{K_R/2}\mathcal{F}(\gamma)\right], \quad (13)$$

where

$$\mathcal{F}(\gamma) = \frac{\sin\gamma \sin 3\gamma + 3\cos\gamma\cos 3\gamma}{2(9 - 8\sin^2 3\gamma)^{1/2}}. \quad (14)$$

The eigenvectors $a^I_{q,K}$ are obtained by diagonalizing the Hamiltonian (1). The $|U^f_q|^2$ is the probability that the proton single-particle state in the daughter nucleus is empty. The quantity $\phi^{q\Omega}_{lj}(r)$ is the radial component of the single-particle wave function. F and G are regular and irregular Coulomb wave functions, respectively.

The total decay width is obtained by summing these partial decay widths over all the possible combinations of l and j values and hence,

$$\Gamma^{IR} = \sum_{j=|R-I|}^{j=R+I} \Gamma^{IR}_{lj}. \quad (15)$$

The half-lives are obtained using the expression $T_{1/2} = \hbar \ln 2/\Gamma$. The full description of decay width and half-life is given in Refs. [17–19].

III. RESULTS AND DISCUSSIONS

We have applied the above formalism to study the structure and decay properties of ^{109}I. The deformation parameters $\beta_2 = 0.16$, $\beta_4 = 0.06$, and $\gamma = 10^\circ$ are predicted for ^{109}I according to the macroscopic-microscopic calculations [14,27]. A moderate quadrupole deformation $\beta_2 = 0.143$ ($\beta_4 = 0.04$) and triaxiality $\gamma = 10^\circ$ are suggested by cranking calculations and an analysis with experimental spectra suggests a predominant $\pi g_{7/2}$ configuration for the ground-state band [10]. To ascertain the deformation, we start our calculations with the rotational spectrum of the daughter nucleus ^{108}Te. Since the experimental value of the first 2^+ excitation energy E^+_2 of ^{108}Te is 652.2 keV [26], using the Grodzins empirical formula [28], a quadrupole deformation $\beta_2 = 0.18$ can be obtained. The rotor ^{108}Te also exhibits the quadrupole vibration [29] and octupole collectivity [26,30]. In such cases, the rotational spectrum is quite compressed when compared to a rigid-rotor spectrum. Alternatively, such a spectrum can be obtained within a rotor formalism but with a high γ value. For analyzing the triaxial deformation γ for ^{108}Te, we obtain the ground-state rotational spectrum through the VMI models.

In Fig. 1, the rotor energies shown are calculated by using two methods given by Eqs. (6) and (7). The results of the parameter b dependent VMI clearly indicate that the data can be explained only with a large γ. However, the results from this method are very sensitive to b and γ, but one may not get a good fit [Fig. 1(a)] when there is a strong influence of a vibration. A better fit is achieved by the other VMI model where the vibrational degrees of freedom are taken care of in a simple way through the parameters C and $\mathcal{I}_0$ of Eq. (6). For the best fitting case, we get $\gamma = 30^\circ$. The parameter $\mathcal{I}_0$ can have a negative value also as depicted in the figure, but it always yields

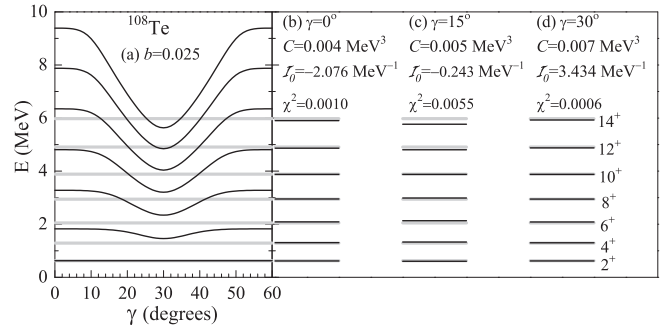

FIG. 1. Energy spectrum of ^{108}Te calculated with different triaxial deformations compared with the experimental data [26] represented by grey lines. In the case (a), the variable moment of inertia (VMI) is represented by the parameter b [Eq. (7)]; for (b)–(d) the VMI is represented by the parameters C and $\mathcal{I}_0$ [Eq. (6)]. The magnitude of the axial deformation (β_2) is contained in the energy of the 2^+ state which is taken as a reference here.

a positive moment of inertia ($\mathcal{I}_{kRi}$). The negative value of $\mathcal{I}_0$ increases the potential energy term [Eq. (6)] which corresponds to the vibrational degrees of freedom. This entails that if one wants a good fit for ^{108}Te at zero or low γ, the vibration like component will increase. In this model, the role of γ is crucial only for the γ band, for which the data are not available. Hence the fit is visibly good at all the γ (0°, 15°, and 30°) and the χ^2 value is least for $\gamma \sim 30^\circ$. When the vibrations are not taken care of properly, we have a good fit with large γ only [as seen in Fig. 1(a)]. On the other hand when vibrations are taken care of in a better way, we have a reasonable fit independent of the choice of γ [as seen in Figs. 1(b)–1(d)]. This allows us to conclude that either the vibrational or the triaxial degrees of freedom play a very vital role in ^{108}Te because the spectrum deviates significantly from that of an axially deformed rotor. The spectrum of ^{108}Te does not allow us to determine the value of γ, but the spectrum of ^{109}I may carry this signature.

To analyze the properties of ^{109}I, rotational spectra are calculated by the coupling of the valence proton with the rotor as discussed in the formalism. These calculations are based on the single-particle and quasiparticle states which are presented in Fig. 2. Figures 2(a) and 2(b) show these energies as a function of the quadrupole deformation β_2 ($\gamma = 0^\circ$) and Figs. 2(c) and 2(d) are with respect to the triaxial deformation γ. The relation between β_4 and β_2 is taken to satisfy the β_4 and β_2 predicted in Ref. [27]. Esbensen-Davids' set of parameters [31] are utilized in the mean-field calculations with a triaxially deformed Woods-Saxon potential. From Fig. 2(a), we can observe that the valence proton is in the state $\Omega = 3/2$ of the $d_{5/2}$ orbital till $\beta_2 \sim 0.1$ and then in the state $\Omega = 1/2$ of the $g_{7/2}$ orbital up to $\beta_2 \sim 0.2$. In an adiabatic approach, the band head (decaying state) can be any of the valence Nilsson state [6]. But in the nonadiabatic approach the band heads are a mixture of Nilsson states interacting with each other through the Coriolis interaction. In the single-particle representation, the levels near the valence orbital [denoted by green dashed line in Fig. 2(a)] can contribute significantly to the ground state. The quasiparticle representation takes care of the proximity to the chemical potential [through the term $(e_q - \lambda)$ in Eq. (9)]

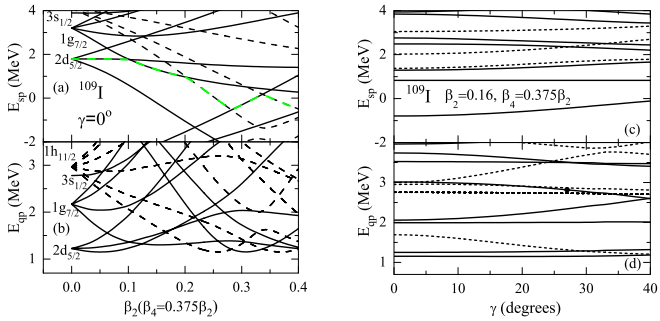

FIG. 2. Single-particle and quasiparticle energies of ^{109}I as a function of deformation parameters β_2 and γ, calculated with the Esbensen-Davids set of parameters [31]. The choice of β_2 and β_4 are consistent with the finite-range droplet model calculations [27]. The solid and dashed lines correspond to the positive and negative parity states, respectively. The green dashed line represents the states of the valence particle. At zero deformation the degenerate states are labeled by the quantum numbers nl_j.

and hence the valence level comes out to be the lowest in energy. From Fig. 2(c), we can identify that the single-particle energy levels are not very sensitive to γ. In the quasiparticle representation [Fig. 2(d)], one can identify subtle changes in the level ordering beyond $\gamma \gtrsim 20^\circ$. However, the lower lying states are almost unaffected by γ. For $\beta_2 = 0.16$ and positive parity, the two levels with $\Omega = 3/2$ from $d_{5/2}$ and $\Omega = 1/2$ from $g_{7/2}$ contribute significantly to the positive parity band irrespective of γ, but many other neighboring levels also contribute substantially with the change in β_2. For negative parity, it is obvious that the major contribution is from levels of the $h_{11/2}$ orbital. These levels identified to be relevant are considered as the basis for the rotation particle coupling calculations for the particle-plus-rotor system.

For the calculation of negative parity angular momentum states of ^{109}I, we have included all the levels of the $h_{11/2}$ orbital. Another input for our calculations are the energies of the rotor which are available experimentally up to $R^\pi = 14^+$. Beyond this angular momentum, the rotor energies calculated through the VMI model (6) are used. In Fig. 3(a), the measured band built on the negative parity isomeric state of ^{109}I is shown along with the calculated results. The rotational state with $I^\pi = 11/2^-$ has a dominant contribution from the negative parity valence level having $\Omega = 1/2$ originating from the $h_{11/2}$ orbital [Fig. 2(a)]. This is a good example of rotation alignment leading to a decoupled band where the states with $I^\pi = 13/2^-, 17/2^-, 21/2^-, \ldots$ lie higher in energy. From Fig. 3(a), we can say that the negative parity spectrum of ^{109}I has a good agreement with the data at lower triaxial deformations ($\gamma \lesssim 15^\circ$). The spectrum looks less sensitive to γ, because most of the role of γ deformation is already built in the experimental core energies which are provided as input for these calculations. For the particle-plus-rotor system, if one employs a rigid rotor or a simple VMI model [like the one given by Eq. (7)] where the rotor energies also change significantly with γ, then the spectrum would be very sensitive to γ.

For the positive parity spectrum, all the single-particle levels originating from the $1g_{9/2}$, $2d_{5/2}$, and $1g_{7/2}$ orbitals are included. When we count the positive parity levels from the bottom ($1s_{1/2}$) of the energy level diagram, the lowest energy level of $2d_{5/2}$ orbital is the 13th positive parity level while $\beta_2 \to 0$. In our calculations, we achieve convergence at all the considered deformations, while considering the 11th to 19th positive parity levels which include the single-particle levels of $1g_{9/2}$, $2d_{5/2}$ and $1g_{7/2}$ orbitals. It has to be noted that for the triaxial case, Ω is not a good quantum number and hence it cannot be used to label the single-particle levels. In such cases, we employ the counting from the bottom to index these energy levels. In Fig. 3(b) the calculated positive parity band along with the data are shown. Similar to the negative parity band, the positive parity band is also not very sensitive to the γ deformation. Both the positive and negative parity bands of ^{109}I agree well with the data at the same β_2. The calculated positive parity spectrum has a good agreement with the data for a wide range of γ but the fit is better for the range $15^\circ \lesssim \gamma \lesssim 25^\circ$. This band turns out to be built on the $I = 7/2^+$ state in the range $0.04 \lesssim \beta_2 \lesssim 0.24$ where the agreement is good as shown in Fig. 3(c). After $\beta_2 \sim 0.25$, the level ordering changes with the $11/2^+$ state coming down. The abrupt change in the energies for larger deformation is coming from the $\Omega = 9/2$ of the $1g_{9/2}$ that is crossing the Fermi energy [green dashed line in Fig. 2(a)]. This gives a band starting with $I^\pi = 9/2^+$ that becomes lower than the band starting with $I^\pi = 7/2^+$ that was the yrast at lower deformation. The results in Fig. 3(c) is presented in a different form in Fig. 4, along with the data of the ground band in ^{108}Te. In rotation-particle coupling calculations, when $\beta_2 \to 0$, the low-lying one-quasiparticle bands match the ground band of

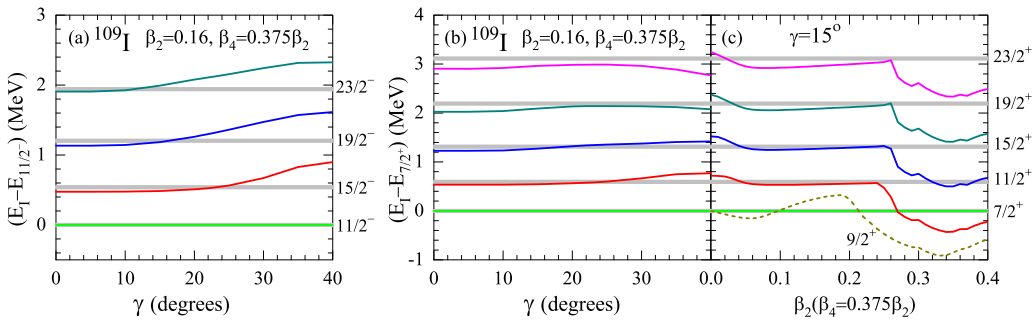

FIG. 3. Negative parity band (a) and positive parity band [(b) and (c)] of ^{109}I are shown as functions of deformation parameters. The grey lines indicate the experimental data [10,13].

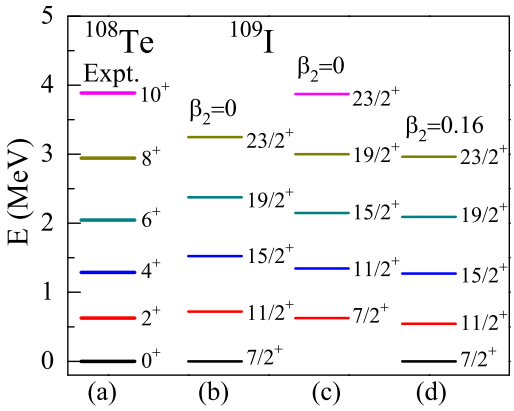

FIG. 4. Experimental data of the ground band in ^{108}Te [26] (a) and the calculated positive parity band of ^{109}I at quadrupole deformations $\beta_2 = 0$ [(b) and (c)] and $\beta_2 = 0.16$ ($\beta_4 = 0.375\beta_2$) (d) are shown here. (b) and (c) represent the same results but the energy of the $7/2^+$ state of ^{109}I is matched with the 0^+ and 2^+ states, respectively, in ^{108}Te.

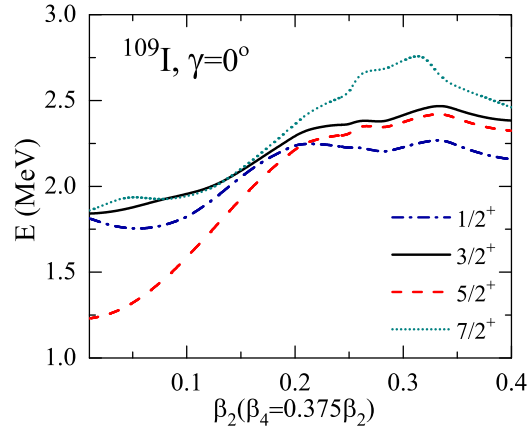

FIG. 5. Yrast states of ^{109}I calculated with the parameters of [31] are shown as a function of β_2 at $\gamma = 0^\circ$.

the rotor. As shown in Fig. 4(b), the above criterion is not satisfied for the positive parity band in ^{109}I if we assume the band to be built on the $7/2^+$ state. But as shown in Fig. 4(c), if we assume the band to be built on the $5/2^+$ state, then the energies of $7/2^+$, $11/2^+$, $15/2^+$, ... match the rotor energies corresponding to the 2^+, 4^+, 6^+, ..., respectively. Thus, while $\beta_2 \to 0$, the positive parity band in ^{109}I has the configuration of $2d_{5/2}$, at a larger deformation, e.g. at $\beta_2 = 0.16$ as shown in Fig. 4(d), we can interpret the band to be built on the $g_{7/2}$ state. It is known [32] that the energies of decoupled band are not very sensitive to the β_2 deformation for moderate prolate deformations. Hence, in Fig. 4(d), the energies of $7/2^+$, $11/2^+$, $15/2^+$, ... match the rotor energies corresponding to the 0^+, 2^+, 4^+, ..., respectively. This match is valid in a wider range where $0.04 \lesssim \beta_2 \lesssim 0.24$ as shown in Fig. 3(c).

According to the systematics presented in Ref. [10], the $5/2^+$ state lies very close to the $7/2^+$ state and hence it is difficult to predict the exact ground state. The results in Ref. [6] also suggest that the ground state is a positive parity state below the $7/2^+$ state. The positive parity energy levels with energies lesser or equal to that of the $7/2^+$ state are shown in Fig. 5 as a function of β_2. At zero deformation, the lowest energy state is $5/2^+$ and other states $1/2^+$ and $3/2^+$ are almost degenerate with the $7/2^+$ with the spacing from the $5/2^+$ equal to the E_{2+} of the rotor. This degeneracy and spacing indicates that these levels correspond to the coupling between $R = 2$ and $j = 5/2$ ($2d_{5/2}$). In other words, at $\beta_2 \sim 0$, the states $1/2^+$, $3/2^+$, and $7/2^+$ are built on the state $5/2^+$ which turns out to be the ground state at lower deformation. As the deformation increases, the drastic deviation of this spacing from the E_{2+} of the rotor indicates that the contribution from the $1g_{7/2}$ increases significantly. At larger deformations of our interest ($\beta_2 \sim 0.16$), the contribution to $7/2^+$ state from the $2d_{5/2}$ should be substantially less than the contribution at zero deformation. The ordering of levels changes considerably with the deformation. For $\beta_2 \sim 0.16$ the energy separation between different states are not very large and hence these states have similar probability of being the ground state.

We present in Fig. 6, the contribution of various single-particle angular momentum (j) to the state $I^\pi = 7/2^+$ of the particle-plus-rotor system as a function of β_2 (β_4). At smaller β_2, the maximum contribution is from $j = 5/2$ ($d_{5/2}$). As the deformation increases, the contribution from $j = 7/2$ ($g_{7/2}$) increases and $j = 5/2$ ($d_{5/2}$) decreases. At $\beta_2 = 0.16$ the contributions from $j = 5/2$ and $7/2$ are nearly equal. At higher deformations, $j = 9/2$ ($g_{9/2}$) becomes dominant. Thus we can observe that the lowest positive parity state has $j = 5/2$ at very low β_2, at moderate deformations there is a strong admixture of $1g_{7/2}$ and $2d_{5/2}$ states, and at very high deformations $j = 9/2$ becomes the most prominent. In Ref. [10], the positive parity band is proposed to be associated with the $\pi g_{7/2}$ orbital (supported by cranking calculations also) but the relative placement of $5/2^+$ and $7/2^+$ is uncertain.

Utilizing the wave functions of the particle-plus-rotor system (^{109}I), we calculate the proton emission half-lives. The results with the Esbensen-Davids parameter set is presented in Fig. 7. The comparison between experimental and theoretical proton-decay half-lives using a deformed single-particle Nilsson model [6] suggests that the ground state could be a $1/2^+$ or $3/2^+$ state decaying by proton emission. From ^{109}I,

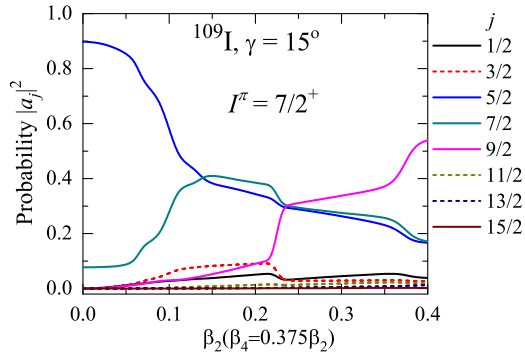

FIG. 6. Probability density of different single-particle angular momentum (j) states $|a_j|^2$ in the $I^\pi = 7/2^+$ state of ^{109}I as a function of β_2 (β_4) at $\gamma = 15^\circ$.

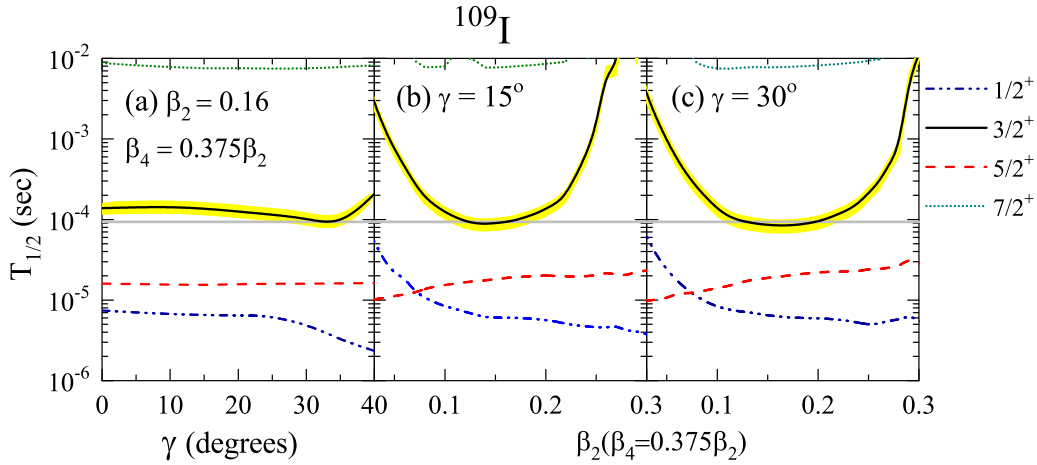

FIG. 7. Half-life of proton emission from the the yrast states of ^{109}I shown with the parameter set in [31] as a function of deformation parameters (a) γ, (b) β_2 at $\gamma = 30°$, and (c) β_2 at $\gamma = 15°$. The grey line corresponds to the experimental half-life [3,33] with its width representing the uncertainty in data. The yellow area represents the possible error in the calculated half-life due to the uncertainty in the experimental values of Q_p [34] used as an input in our calculations.

proton decays to the ground state of the daughter nucleus. If the proton is emitted from the ground state of the parent nucleus, then from the half-life calculation we can find the proton emitting state which will be the ground state also. In Fig. 7(a), the calculated half-lives of different angular momentum states are shown as functions of γ, at a fixed $\beta_2(\beta_4)$ [27]. In the Figs. 7(b) and 7(c), γ is fixed at 15° and 30°, respectively and the half-life is calculated as a function of $\beta_2(\beta_4)$. Here the half-life calculated from the $7/2^+$ state is much higher than the measured half-life. The half-lives of $1/2^+$ and $5/2^+$ are far from the data by an order of magnitude. The angular momentum state $3/2^+$ yields the proton emission half-life conforming the data [3,33]. Figure 7(a) suggests that the half-life is not very sensitive to γ deformation and the half-life of $5/2^+$ is quite independent of γ. From Figs. 7(b) and 7(c), we observe that only for $\beta_2 \sim 0.16$ (with $\beta_4 = 0.375\beta_2$ consistent with macroscopic-microscopic calculations [27]) the calculated results could explain the data.

To check the impact of the parameters of the mean-field potential on the above inference, we repeated our calculations with Chepurnov's parameters [35]. These results (not shown here) are similar to those obtained with the Esbensen-Davids parameters. The major difference between the two parameter sets is the strength of the spin-orbit potential.

IV. SUMMARY

To understand the structure of ^{109}I through the phenomenon of proton emission, we have performed calculations with a nonadiabatic quasiparticle approach with the inclusion of the triaxial degree of freedom. We observe that either the vibrational or triaxial degrees of freedom play a very vital role in ^{108}Te because the spectrum deviates significantly from that of an axially deformed rotor. This argument can be carried forward to ^{109}I, since the core energies (^{108}Te) are taken as input, while studying the properties of ^{109}I. We get a good fit for both the positive and negative parity bands of ^{109}I with the same set of deformation parameters. We find that the positive parity band has strong admixture of $1g_{7/2}$ and $2d_{5/2}$ states. The configuration for the negative parity band is predominantly $1h_{11/2}$. In ^{109}I, the comparison of calculated proton emission half-lives with data enables us to conclude that the proton is emitted from the $3/2^+$ state originating from the admixture of $1g_{7/2}$ and $2d_{5/2}$ states.

ACKNOWLEDGMENT

This work is supported by the Council of Scientific and Industrial Research, Government of India, via Project No. 03(1338)/15/EMR-II.

[1] T. Faestermann, A. Gillitzer, K. Hartel, P. Kienle, and E. Nolte, Phys. Lett. B **137**, 23 (1984).
[2] P. J. Sellin, P. J. Woods, T. Davinson, N. J. Davis, K. Livingston, R. D. Page, A. C. Shotter, S. Hofmann, and A. N. James, Phys. Rev. C **47**, 1933 (1993).
[3] C. Mazzocchi, R. Grzywacz, S. N. Liddick, K. P. Rykaczewski, H. Schatz, J. C. Batchelder, C. R. Bingham, C. J. Gross, J. H. Hamilton, J. K. Hwang *et al.*, Phys. Rev. Lett. **98**, 212501 (2007).
[4] V. P. Bugrov and S. G. Kadmensky, Sov. J. Nucl. Phys. **49**, 967 (1989).
[5] P. Möller, R. J. Nix, and K. L. Kratz, At. Data Nucl. Data Tables **66**, 131 (1997).
[6] E. Maglione, L. S. Ferreira, and R. J. Liotta, Phys. Rev. C **59**, R589(R) (1999).
[7] B. Barmore, A. T. Kruppa, W. Nazarewicz, and T. Vertse, Phys. Rev. C **62**, 054315 (2000).
[8] G. Lalazissis, D. Vretenar, and P. Ring, Nucl. Phys. A **650**, 133 (1999).
[9] A. Gillitzer, T. Faestermann, K. Hartel, P. Kienle, and E. Nolte, Z. Phys. A **326**, 107 (1987).

[10] M. Petri, E. S. Paul, B. Cederwall, I. G. Darby, M. R. Dimmock, S. Eeckhaudt, E. Ganioglu, T. Grahn, P. T. Greenlees, B. Hadinia *et al.*, Phys. Rev. C **76**, 054301 (2007).
[11] E. S. Paul, P. J. Woods, T. Davinson, R. D. Page, P. J. Sellin, C. W. Beausang, R. M. Clark, R. A. Cunningham, S. A. Forbes, D. B. Fossan *et al.*, Phys. Rev. C **51**, 78 (1995).
[12] C.-H. Yu, A. Galindo-Uribarri, S. D. Paul, M. P. Carpenter, C. N. Davids, R. V. F. Janssens, C. J. Lister, D. Seweryniak, J. Uusitalo, and B. D. MacDonald, Phys. Rev. C **59**, R1834 (1999).
[13] M. G. Procter, D. M. Cullen, C. Scholey, P. Ruotsalainen, L. Angus, T. Bäck, B. Cederwall, A. Dewald, C. Fransen, T. Grahn *et al.*, Phys. Lett. B **704**, 118 (2011).
[14] P. Möller, R. Bengtsson, B. Carlsson, P. Olivius, T. Ichikawa, H. Sagawa, and A. Iwamoto, At. Data Nucl. Data Tables **94**, 758 (2008).
[15] S. Modi, M. Patial, P. Arumugam, E. Maglione, and L. S. Ferreira, Phys. Rev. C **95**, 024326 (2017).
[16] K. T. Hecht and G. R. Satchler, Nucl. Phys. **32**, 286 (1962).
[17] P. Arumugam, E. Maglione, and L. S. Ferreira, Phys. Rev. C **76**, 044311 (2007).
[18] P. Arumugam, L. S. Ferreira, and E. Maglione, Phys. Rev. C **78**, 041305 (2008).
[19] P. Arumugam, L. S. Ferreira, and E. Maglione, Phys. Lett. B **680**, 443 (2009).
[20] W. Greiner and J. A. Maruhn, *Nuclear Models* (Springer-Verlag, Berlin, 1996).
[21] H. Toki and A. Faessler, Z. Phys. A **276**, 35 (1976).
[22] M. A. J. Mariscotti, G. Scharff-Goldhaber, and B. Buck, Phys. Rev. **178**, 1864 (1969).
[23] G.-j. Chen, Y.-x. Liu, H.-c. Song, and H. Cao, Phys. Rev. C **73**, 034304 (2006).
[24] A. S. Davydov and G. F. Filippov, Nucl. Phys. **8**, 237 (1958).
[25] G. Fiorin, E. Maglione, and L. S. Ferreira, Phys. Rev. C **67**, 054302 (2003).
[26] G. J. Lane, D. B. Fossan, J. M. Sears, J. F. Smith, J. A. Cameron, R. M. Clark, I. M. Hibbert, V. P. Janzen, R. Krücken, I.-Y. Lee *et al.*, Phys. Rev. C **57**, R1022(R) (1998).
[27] P. Möller, J. R. Nix, W. D. Myers, and W. J. Swiatecki, At. Data Nucl. Data Tables **59**, 185 (1995).
[28] L. Grodzins, Phys. Lett. **2**, 88 (1962).
[29] B. Hadinia, B. Cederwall, J. Blomqvist, E. Ganioglu, P. T. Greenlees, K. Andgren, I. G. Darby, S. Eeckhaudt, E. Ideguchi, P. M. Jones *et al.*, Phys. Rev. C **72**, 041303(R) (2005).
[30] E. S. Paul, A. O. Evans, A. J. Boston, C. J. Chiara, M. Devlin, D. B. Fossan, S. J. Freeman, D. R. LaFosse, G. J. Lane, M. J. Leddy *et al.*, Phys. Rev. C **76**, 034323 (2007).
[31] H. Esbensen and C. N. Davids, Phys. Rev. C **63**, 014315 (2000).
[32] F. S. Stephens, Rev. Mod. Phys. **47**, 43 (1975).
[33] B. Blank and M. Borge, Prog. Part. and Nucl. Phys. **60**, 403 (2008).
[34] B. Blank and M. Płoszajczak, Rep. Prog. Phys. **71**, 046301 (2008).
[35] V. A. Chepurnov, Yadern. Fiz. **6**, 955 (1967).